Brazilian Journal of Physics (2022) 52:164
https://doi.org/10.1007/s13538-022-01166-9

CONDENSED MATTER

# Singlet Oxygen Generation and Spectroscopic Properties of Supramolecular Zinc *Meso*-tetra(4-pyridyl) Porphyrin Bearing Outlying Ruthenium Groups

J. M. S. Lopes[1] · S. N. Costa[1,2] · E. Silveira-Alves Jr[3] · A. A. Batista[4] · L. R. Dinelli[5] · P. J. Gonçalves[3,6] · P. T. Araujo[7] · N. M. Barbosa Neto[1]

Received: 27 April 2022 / Accepted: 13 July 2022


**Abstract**
Here, we investigate the effects introduced in the spectroscopic properties and singlet oxygen generation efficiency of zinc tetra(4-pyridyl) porphyrin (ZnTPyP) when the molecule undergoes outlying decoration with the $[RuCl_2(PPh_3)_2(CO)(DMF)]$ and $[RuCl_2(dppb)(CO)(DMF)]$ ruthenium complexes. Our results show that these metallic compounds can significantly affect the electronic and vibronic B- and Q-bands; the excited-state deactivation processes; and the singlet oxygen generation quantum yield of the porphyrin, being their influence affected by the ligands present in the ruthenium complexes.

**Keywords** Zinc porphyrin · Ruthenium complex · Photophysical properties · Singlet oxygen generation

## 1 Introduction

In the field of molecular sciences, the search for systems with tunable structures and properties is in constant evolution [1–5]. The number of areas is endless, ranging from a great variety of devices [6–8] to photoinduced medical applications [9–11]. Notably, the synthesis of supramolecular structures opens the possibility for emerging properties that only exist due to the combination of two or more molecules [4, 12, 13]. The supramolecular structures allow the exploration of fundamental structure-properties relationships that can be used as a guide for systems with novel characteristics. In this scenario, the use of spectroscopic tools to investigate molecules is well established and allows us to obtain a big picture of how structural parameters affect vibronic progressions [14], hot fluorescence [15], excited-state relaxations [16], and excited triplet state formation [17].

Porphyrins, which are macrorings constituted of four pyrrole rings, rise as versatile candidates that can be modified in many ways, e.g., central ring substitution [18–20], *meso*-carbon substitution [21, 22], axial ligand biding [23, 24], dimer or aggregate formation [25–27], and supramolecular structure synthesis [13, 28, 29]. In particular, the decoration of the porphyrins' rings with outlying metal complexes like ruthenium [13] or rhenium [30] complexes offers several possibilities for their technological applications [13, 30–35]. Due to the nature of their cyclic long-length conjugation, porphyrins present rich spectroscopic signatures at the UV–Vis spectral region (B- and Q-bands) [36] that are assigned to specific structural features. These molecules also present well-structured fluorescence bands [36, 37] that are associated with the first and second singlet excited state, and hot fluorescence [15, 38–40].

✉ J. M. S. Lopes
lopesjefferson01@yahoo.com.br

✉ P. T. Araujo
paulo.t.araujo@ua.edu

✉ N. M. Barbosa Neto
newtonfisico@gmail.com

1 Institute of Natural Sciences, Graduate Program in Physics, Federal University of Pará, Belém, PA, Brazil

2 Federal Institute of Education, Science, and Technology of Para, Bragança, PA, Brazil

3 Institute of Chemistry, Federal University of Goiás, Goiânia, GO, Brazil

4 Department of Chemistry, Federal University of São Carlos, São Carlos, SP, Brazil

5 College of Sciences of Pontal, Federal University of Uberlândia, Ituiutaba, MG, Brazil

6 Institute of Physics, Federal University of Goiás, Goiânia, GO, Brazil

7 Department of Physics and Astronomy, University of Alabama, Tuscaloosa, AL, USA

Published online: 27 July 2022

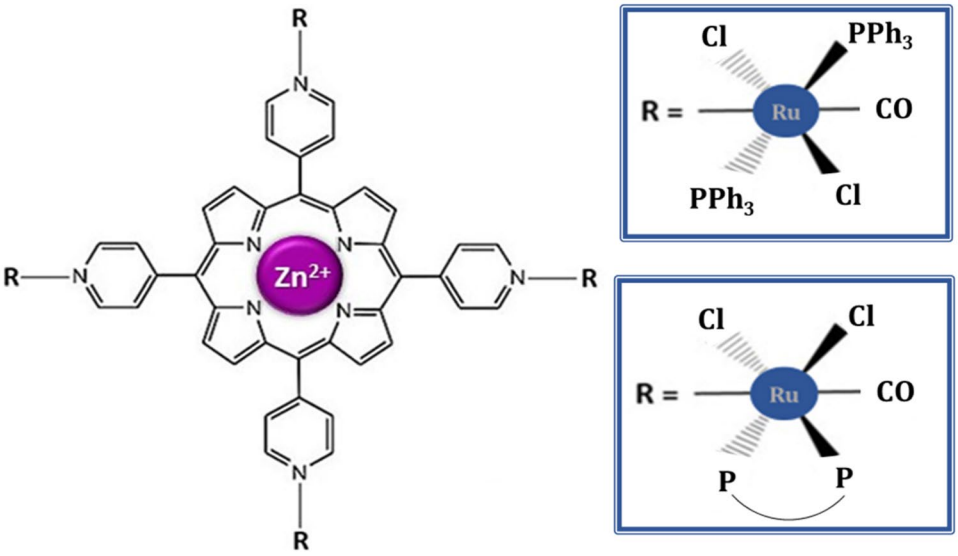


**Scheme 1** Zn(II) 5,10,15,20-*meso*-(4-pyridyl) porphyrin and outlying ruthenium complexes (R). R = [$RuCl_2$(dppb)(CO)] or R = [$RuCl_2(PPh_3)_2$(CO)]. Here, ($PPh_3$) stands for triphenylphosphine and P – P = dppb stands for 1-4-bis-(diphenylphosphine) butane. The ruthenium complexes are bonded to outlying pyridyl groups (**R** sites in the scheme)

Moreover, porphyrins also present accessible excited triplet states due to the presence of strong spin–orbit couplings [36, 37, 41]. This triplet state accessibility makes these molecules good singlet oxygen species generators, turning them into ideal structures to be employed as sensitive drugs in photodynamic therapy (PDT) [11, 42, 43]. Notably, metalloporphyrins have become key systems for PDT [36], since the presence of metal ions in the center of the macrocycle ring leads to the heavy atom effect [44, 45], which enhances the intersystem crossing (ISC) rate [19]. A natural questioning is related to the effects introduced when metal substituents are placed in the outlying positions of the porphyrin ring. In this context, many investigations have been focused on how the outlying metal complexes change the properties of free base porphyrins [32, 44, 46]. However, to the best of our knowledge, the influence of such complexes on the spectroscopic properties of metalloporphyrins is still elusive.

In the present work, we investigated the spectroscopic (absorption and emission) properties and singlet oxygen generation efficiency of supramolecular structures constituted of Zn(II) *meso*-tetra (4-pyridyl) porphyrin (ZnTPyP), and [$RuCl_2$(dppb)(CO)(DMF)] and [$RuCl_2$ ($PPh_3$)$_2$(CO)(DMF)] ruthenium complexes. The structures are formed through the biding of four ruthenium complexes (of each type) at zinc porphyrin's pyridyl moiety, forming ZnTPyP[$RuCl_2$(dppb)(CO)]$_4$, and ZnTPyP[$RuCl_2(PPh_3)_2$(CO)]$_4$, which are novel supramolecular structures containing five metal sites (as shown in Scheme 1). Our results show that the metalloporphyrin singlet oxygen generation's efficiency is tunable according to the type of outlying ruthenium complexes.

## 2 Results and Discussions

### 2.1 Light Absorption

According to the four-orbital model proposed by Martin Gouterman, the UV–Vis spectrum of zinc porphyrins is caused by the cyclic electron delocalization in the porphyrin ring and is assigned to the $\pi \rightarrow \pi^*$ transitions toward the second ($S_0 \rightarrow S_2$) and first ($S_0 \rightarrow S_1$) singlet excited states which account for the characteristic B- (Soret) and Q-bands, respectively [36, 37, 47]. The transition energies (peak center) assigned to these bands are very sensitive to the conjugation length in the porphyrin ring [48]. The outlying decoration of the macrocycle leads to significant modifications of selection rules involved in these transitions reflecting such changes in fluorescence quantum yield, excited-state lifetimes, intersystem crossing rates, etc. [37, 49]. Figure 1 exhibits representative spectra for ZnTPyP dissolved in DMSO (solid black lines) that are compared with their supramolecular equivalents (solid red and solid green lines). The attachment of ruthenium moieties causes the B-band to broaden and redshift, similar to what happens for supramolecular structures derived from the free base porphyrin analog [44, 50, 51]. Taking ZnTPyP as standard, the shift observed for ZnTPyP[$RuCl_2(PPh_3)_2$(CO)]$_4$ is approximately three times greater than the shift observed for ZnTPyP[$RuCl_2$(dppb)(CO)]$_4$ (see Fig. 1a and Table 1). The presence of outlying ruthenium complexes also redshifts, broadens, and favors the absorption magnitude of the Q-Band's electronic transitions (Q(0, 0) bands), see Fig. 1b.

Recently, our group investigated the electronic and vibronic transitions of free-base *meso*-tetra(4-pyridyl)

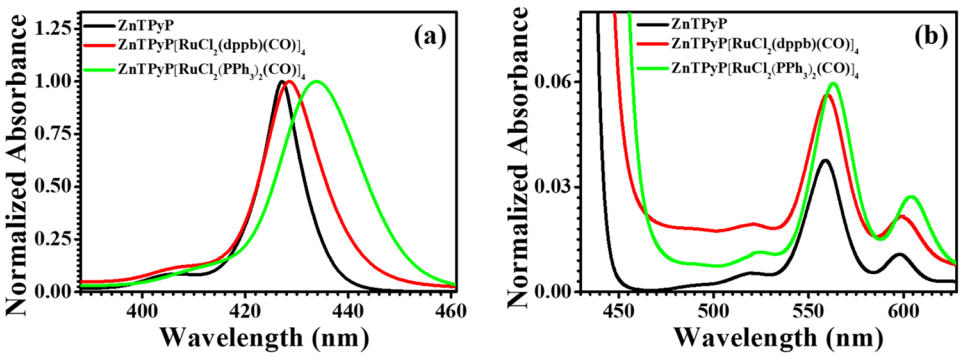


**Fig. 1** Absorbance spectra (normalized at the main B-peak) at the **a** B- and **b** Q- bands of ZnTPyP (solid black line), ZnTPyP[$RuCl_2$(dppb)$(CO)]_4$ (solid red line) and ZnTPyP[$RuCl_2(PPh_3)_2(CO)]_4$ (solid green lines) porphyrins dissolved in DMSO

porphyrins [14] and their metallic species ($Zn^{2+}$, $Cu^{2+}$, $Ni^{2+}$, $Co^{2+}$) [15], mapping the evolution of transitions in their B- and Q-bands due to the change of the ion in the center of the porphyrin ring (central ion). For ZnTPyP, the Q-band presents additional semi-degenerated transitions that comprise two $Q_1$ and $Q_2$ electronic bands along with their respective vibronic components, while the B-band is composed of a B(0,0) electronic transition with a first vibronic transition [15]. It was also observed that when the central ion is changed from $Zn^{2+}$ (closed-shell $d^{10}$ ion) to $Co^{2+}$ (open-shell $d^7$ ion) the porphyrin spectrum presents the following modifications: (i) the B-band shows suppression of the vibronic transition, which can be understood on bases of changes in the absorption selection rules; (ii) the Q-band structuration evolves with a decrease in the contribution of electronic transitions ($Q_1(0,0)$ and $Q_2(0,0)$)

**Table 1** Parameters for B- and Q-bands obtained via the spectral deconvolution in association with derivative analysis of ZnTPyP, ZnTPyP[$RuCl_2$(dppb)$(CO)]_4$, and ZnTPyP[$RuCl_2(PPh_3)_2(CO)]_4$ absorption spectra

| | ZnTPyP | ZnTPyP[RuCl2(dppb)$(CO)]_4$ | ZnTPyP[$RuCl_2(PPh_3)_2(CO)]_4$ |
|---|---|---|---|
| **B-band** | | | |
| $\lambda_{max}(B(0,1))$ | 404 nm | 407 nm | 411 nm |
| $\lambda_{max}(B(0,0))$ | 427 nm | 428 nm | 432 nm |
| $\lambda_{max}(B_x)$ | ------ | 432 nm | 440 nm |
| $\frac{B(0,1)}{B(0,0)}$ | ~0.069 | ~0.063 | ~0.079 |
| $\frac{B_x}{B(0,0)}$ | 0 | ~0.385 | ~0.470 |
| **Q-band** | | | |
| $\lambda_{max}(Q_2(0,2))$ | 519 nm | 521 nm | 522 nm |
| $\lambda_{max}(Q_2(0,1))$ | 549 nm | 549 nm | 551 nm |
| $\lambda_{max}(Q_2(0,0))$ | 582 nm | 581 nm | 584 nm |
| $\lambda_{max}(Q_1(0,1))$ | 560 nm | 559 nm | 563 nm |
| $\lambda_{max}(Q_1(0,0))$ | 598 nm | 599 nm | 605 nm |
| $\frac{Q_2(0,1)}{Q_2(0,0)}$ | ~4.52 | ~4.51 | ~2.85 |
| $\frac{Q_1(0,1)}{Q_1(0,0)}$ | ~4.03 | ~3.79 | ~2.47 |

[15]. These results indicate that the change of the central ion significantly changes the porphyrin symmetry in solution, which are manifested in the absorbance spectra and captured by the method of spectral derivative analysis and deconvolution as described in references [14–16]. By extending these considerations to the supramolecular ZnTPyP, we obtain a more accurate understanding of the role played by the outlying ruthenium complexes on the zinc porphyrins electronic and vibrational properties. In Fig. 2, we show the B-band of ZnTPyP, ZnTPyP[$RuCl_2$(dppb)$(CO)]_4$, and ZnTPyP[$RuCl_2(PPh_3)_2(CO)]_4$, dissolved in DMSO along with the derivative and Voigt deconvolution analysis. It is noted that ZnTPyP present a B-band composed of a main electronic (B(0, 0)) transition located at 427 nm and a vibronic progression located at 404 nm (B(0, 1)). The energy gap between the electronic (0, 0) and first vibronic (1, 0) state of ZnTPyP in DMSO presents very similar structuration when compared to ZnTPyP dissolved in the solvent mixture $CHCl_3$:MeOH (9:1 v/v) [15].

Regarding the absorbance spectrum, it is known that the substitution of different moieties at the *meso*-carbons of the macrocyclic ring, only results in a small effect in the $\pi \rightarrow \pi^*$ transitions and HOMO-LUMO gap [21, 36]. However, as can be seen from Fig. 2, the addition of outlying ruthenium complexes in each pyridyl site generates additional transitions (blue lines in Fig. 2b, c) in the B-band. A new band, from now on named $B_x$-band, arise at 432 nm for ZnTPyP[$RuCl_2$(dppb)$(CO)]_4$ and at 440 nm for ZnTPyP[$RuCl_2(PPh_3)_2(CO)]_4$. The spectral parameters obtained from the B-band deconvolution are summarized in Table 1.

The origin of $B_x$-band can be assigned to (i) contributions coming from MLCT bands of the ruthenium complexes or (ii) the rise of new transitions due to modifications in absorption selection rules, caused by the change in the porphyrin ring symmetry. Due to MLCT transitions, the presence of ruthenium groups attached at outlying *meso* positions causes an enhancement in the magnitude of the spectrum in the spectral region between the B- and Q-bands. In the case of free base tetrapyridyl porphyrin, this enhancement

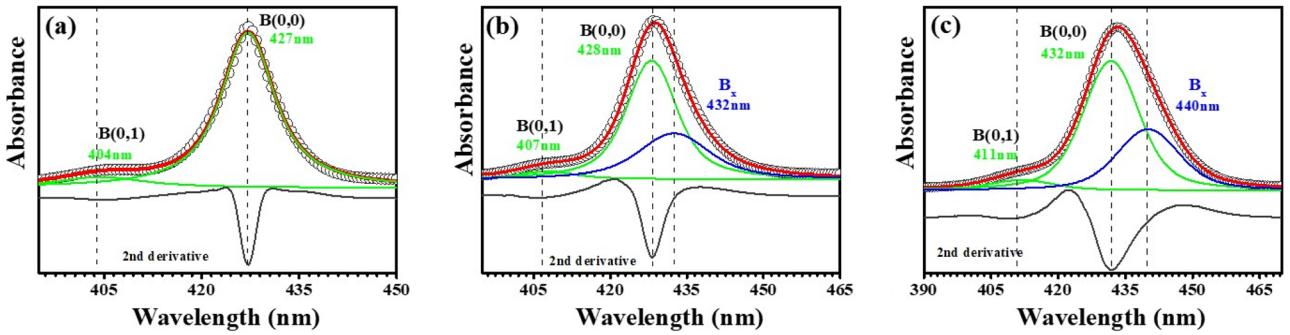


**Fig. 2** B-band deconvoluted spectra for **a** ZnTPyP, **b** ZnTPyP[$RuCl_2$(dppb)(CO)]$_4$, and **c** ZnTPyP[$RuCl_2(PPh_3)_2(CO)]_4$ dissolved in DMSO. The open circles stand for experimental spectra, and the solid red lines represent the fitting results. The solid green and blue lines represent individual Voigt functions. The spectra in solid gray lines are the absorbance second derivative. The Voigt functions represented by the blue solid line in **b** and **c** are assigned to the new $B_x$ band that arises due to the presence of the outlying ruthenium groups

results from a simple superposition of the porphyrin spectrum and the spectra from the four ruthenium complexes' moieties [51]. Here, the same enhancement is observed for tetraruthenated ZnTPyP, see Fig. 1b. However, while the presence of MLCT bands modifies the magnitude of the spectral region between the B- and Q-bands, no influence is observed in the B-band [51]. Furthermore, no direct correlation is observed between the magnitude of the $B_x$ sub-band (blue lines in Fig. 2b, c) and the magnitude of absorbance in the spectral region between B-band and Q -band (Fig. 1b). In one hand, the magnitude of $B_x$-band for ZnTPyP[$RuCl_2$(dppb)(CO)]$_4$ is just ~0.76 times the value of the $B_x$-band observed for ZnTPyP[$RuCl_2(PPh_3)_2(CO)]_4$. On the other hand, in the region between the B- and Q-bands, the magnitude of the spectrum for ZnTPyP[$RuCl_2$(dppb)(CO)]$_4$ is around two times greater than the observed for ZnTPyP[$RuCl_2(PPh_3)_2(CO)]_4$, (compare Figs. 1 and 2). These observations suggest that the rise of the $B_x$-band in these supramolecular structures is not associated with the ruthenium complexes' MLCT bands, supporting the hypothesis that such outlying groups are breaking the ZnTPyP's symmetry and favoring new transitions in the B-band spectral region. This interpretation agrees with recently reported results showing that the multi-structuration of the porphyrin's absorbance spectrum depends on the symmetry of the porphyrin's ring indeed [14–16, 21].

The Q-band of both pristine and supramolecular ZnTPyP are fitted with five Voigt curves that represent the $Q_1$ and $Q_2$ electronic transitions with their respective vibronic progressions see Fig. 3.

The values of spectroscopic parameters obtained from deconvolution of Q-bands are also summarized in Table 1, and significant differences in the relative intensities and energy band gaps due to the attaching of the outlying ruthenium complexes are observed. It is shown that ruthenium complexes distinctly affect the $Q_1\,(Q_2)$ transitions causing blueshifts of ~3.46 meV (~3.67 meV) for ZnTPyP[$RuCl_2$(dppb)(CO)]$_4$ and redshifts of ~23.9 meV (~7.3 meV), for ZnTPyP[$RuCl_2(PPh_3)_2(CO)]_4$ electronic transitions. The changes in the relative intensities of all the Q sub-bands seem to relate to modifications in the equilibrium positions of the excited state potential energy surfaces

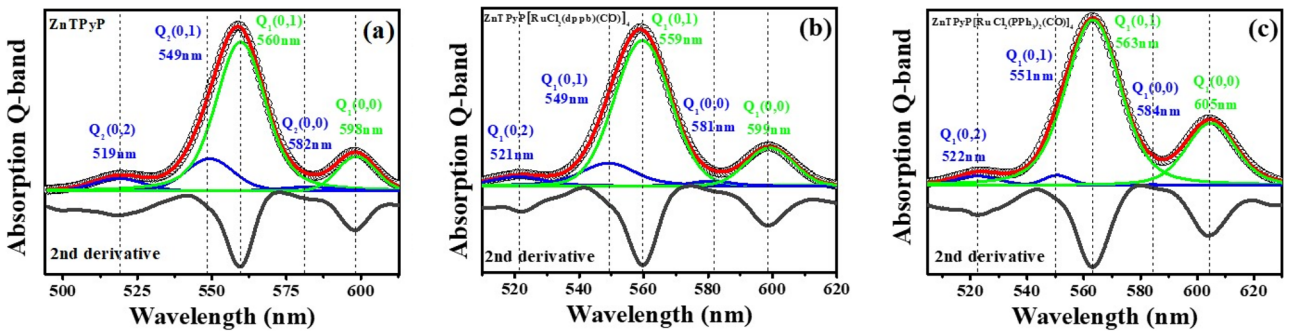


**Fig. 3** Q-band deconvoluted spectra for **a** ZnTPyP, **b** ZnTPyP[$RuCl_2$(dppb)(CO)]$_4$, and **c** ZnTPyP[$RuCl_2(PPh_3)_2(CO)]_4$ dissolved in DMSO. The open circles stand for experimental spectra, and the solid red lines represent the fitting results. The solid green ($Q_1$-bands) and blue ($Q_2$-bands) lines represent individual Voigt functions. The spectra in solid gray lines are the absorbance second derivative

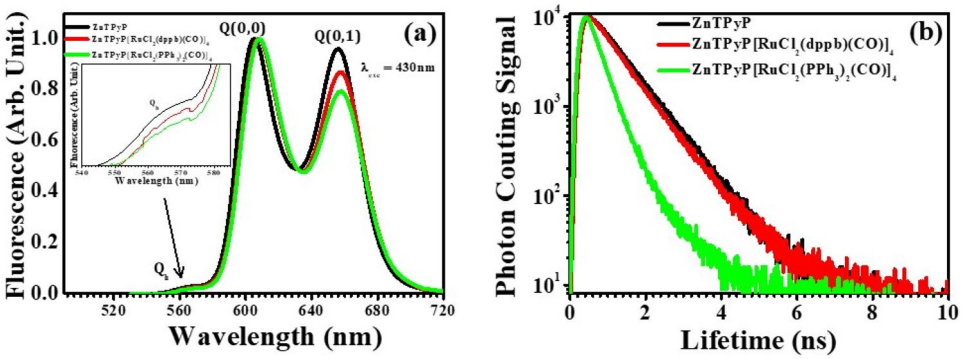


**Fig. 4** **a** Steady-state fluorescence and **b** time-resolved fluorescence acquired for ZnTPyP (black solid lines), ZnTPyP[$RuCl_2$(dppb)(CO)]$_4$ (red solid lines), and ZnTPyP[$RuCl_2(PPh_3)_2$(CO)]$_4$ (green solid lines) dissolved in DMSO. The fluorescence spectra in **a** were acquired by exciting the samples at 430 nm. The fluorescence decay curves in **b** were acquired exciting the samples at 352 nm and probing the signal at 608 nm. The inset in **a** highlights the hot-luminescence spectral bands

(PES). Such modifications are associated with changes in the dipole strength of each vibronic transition which can be estimated via the Huang-Rhys factor $\frac{Q_i(0,0)}{Q_i(0,n)}$, where i = 1, 2 stands for the electronic transition and n is the final vibrational state in the respective vibronic transition [52, 53]. Table 1 presents the intensity ratios extracted from the spectral deconvolution data. These ratios support that all vibronic progressions in the supramolecular structure are distinctly affected, being the increase in the magnitude of electronic transitions favored by the presence of ruthenium complexes.

## 2.2 Fluorescence Emission and Decay

We investigate the ZnTPyP, ZnTPyP[$RuCl_2$(dppb)(CO)]$_4$, and ZnTPyP[$RuCl_2(PPh_3)_2$(CO)]$_4$ fluorescence responses and their excited-state deactivation processes. Steady-state and time-resolved fluorescence from ZnTPyP and their supramolecular counterparts (see Fig. 4) show multi-structured Q(0, 0)- and, Q(0, 1)- bands, and a very weak band located at around 565 nm that is assigned to a hot luminescence process $\left(Q_h\right)$ [15, 16]. Next, to acquire more information on the deactivation pathways, we study the fluorescence spectra using the spectral deconvolution analysis (see Fig. 5).

Comparing the fluorescence spectrum of ZnTPyP dissolved in DMSO (dipole moment 3.96D) with the fluorescence spectrum of ZnTPyP dissolved in $CHCl_3$:MeOH (9:1 v/v) (dipole moment 1.04D:1.70D) [15], it is observed that the $\frac{Q(0,0)}{Q(0,1)}$ intensity ratio increases with increasing solvent polarity. Moreover, the presence of the outlying ruthenium complexes causes small redshifts in $Q_1(0, 0)$, $Q_2(0, 0)$, $Q_1(0, 1)$, and $Q_2(0, 1)$-bands, which is fully correlated with the redshift observed for the $Q_1(0, 0)$ and $Q_2(0, 0)$ absorption bands shown in Fig. 3b. This is understood in terms of Kasha's rule: every emission from the first excited singlet state originates from radiative deactivation of these $Q_{x1}(0,0)$ and $Q_{x2}(0,0)$ low-energy bands [14, 52, 53]. Additionally, the ruthenium groups activate the photoluminescence decay via the $Q_2(0, 1)$ vibronic transition, disfavoring, therefore, the hot-luminescence process previously observed (see inset in Fig. 4a).

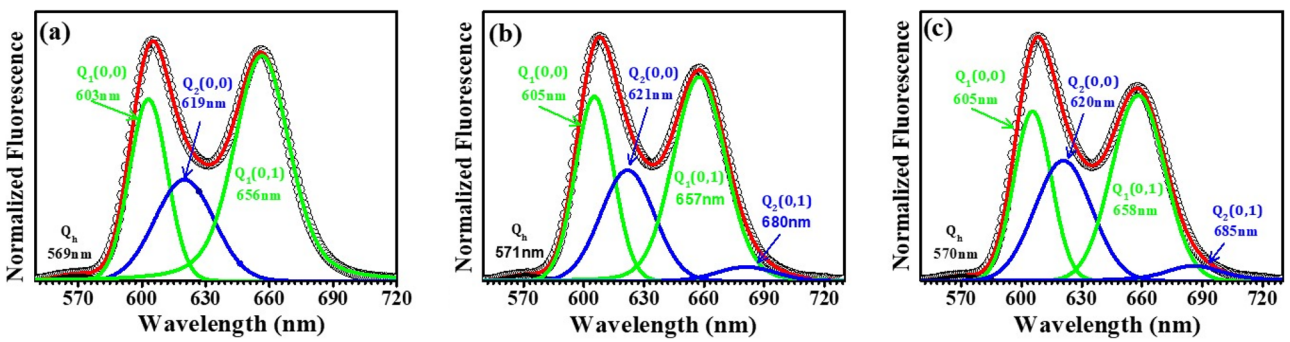


**Fig. 5** Deconvoluted fluorescence spectra for **a** ZnTPyP, **b** ZnTPyP[$RuCl_2$(dppb)(CO)]$_4$, and **c** ZnTPyP[$RuCl_2(PPh_3)_2$(CO)]$_4$ dissolved in DMSO. The open circles stand for experimental spectra, the solid red lines represent the resultant fitting. The solid green ($Q_1$-bands) and blue ($Q_2$-bands) lines represent individual Voigt functions. The excitation wavelength is 430 nm

**Table 2** Steady-state and time-resolved fluorescence parameters. The steady-state parameters come from the spectral deconvolution analysis; $\lambda_{max}$(nm) is the band's center position. The $QY_{FL}$ is the emission quantum yield obtained using ZnTPyP as reference; $\tau_i$ ($i=1$, 2) are the excited-state lifetimes. The values in parentheses represent the relative amplitude of the radiative decay

| | ZnTPyP | ZnTPyP[$RuCl_2$(dppb)(CO)]$_4$ | ZnTPyP[$RuCl_2(PPh_3)_2(CO)]_4$ |
|---|---|---|---|
| **Steady state** | | | |
| $\lambda_{max}(Q_h)$ | 569 nm | 571 nm | 570 nm |
| $\lambda_{max}(Q_1(0,0))$ | 603 nm | 605 nm | 605 nm |
| $\lambda_{max}(Q_2(0,0))$ | 619 nm | 621 nm | 620 nm |
| $\lambda_{max}(Q_1(0,1))$ | 656 nm | 657 nm | 658 nm |
| $\lambda_{max}(Q_2(0,1))$ | ------- | 680 nm | 685 nm |
| $QY_{FL}$ | 0.042* | ~0.042 | 0.035 |
| **Time resolved** | | | |
| $\tau_1$(ns) | ~1.79 (100%) | ~1.71 (100%) | ~1.39 (23%) |
| $\tau_2$(ns) | ------- | ------- | ~0.51 (77%) |

*$QY_{FL}$ for ZnTPyP in DMSO obtained from reference [54]

When compared against ZnTPyP [54], the fluorescence quantum yield $(QY_{FL})$ and lifetime ($\tau$) from the tetraruthenated zinc porphyrins present distinct behavior among themselves. Namely, ZnTPyP[$RuCl_2$(dppb)(CO)]$_4$ shows no modifications in its $QY_{FL}$ with a fluorescence lifetime very close to that measured for ZnTPyP, while ZnTPyP[$RuCl_2(PPh_3)_2$(CO)]$_4$ presents a $QY_{FL}$ equivalent to 84% of the ZnTPyP's $QY_{FL}$ [54] and a drastic modification in its relaxation profile that now shows a bi-exponential behavior. This bi-exponential behavior is associated with a new faster relaxation pathway with a relative amplitude of 77%. Although [$RuCl_2(PPh_3)_2$(CO)(DMF)] creates novel relaxation pathways in the supramolecular structure, we observe that the quantum yield of these new pathways is not significant because no evidence for new fluorescence bands is found. All the spectroscopic parameters obtained from the fluorescence spectra and time-resolved decay analyses are summarized in Table 2.

**Table 3** Singlet oxygen quantum yield $(\Phi_\Delta)$ and triplet state lifetime ($\tau_T$) obtained for ZnTPyP, ZnTPyP[$RuCl_2$(dppb)(CO)]$_4$, and ZnTPyP [$RuCl_2$ $(PPh_3)_2$(CO)]$_4$

| | ZnTPyP | ZnTPyP[$RuCl_2$(dppb)(CO)]$_4$ | ZnTPyP[$RuCl_2(PPh_3)_2$(CO)]$_4$ |
|---|---|---|---|
| $\Phi_\Delta$ | 0.09 | 0.07 | 0.16 |
| $\tau_T$(μs) | 153 | 252 | 162 |

The supramolecular ZnTPyP[$RuCl_2(PPh_3)_2$(CO)]$_4$ $QY_{FL}$ evidences that ruthenium complexes are likely facilitating the creation of nonradiative channels for the porphyrin ring, which in turn quenches the ZnTPyP emission. The literature for $H_2$TPyP states that the quenching mechanism associated with the ruthenium complexes is a combination of new internal conversions (IC) [50] with the increasing in the macrocycle intersystem crossing (ISC) rate driven by the heavy-atom effect [44, 46].

## 2.3 Triplet Decay and Singlet Oxygen Generation

The capacity of these supramolecular structures to generate singlet oxygen species is likely affected by the presence of

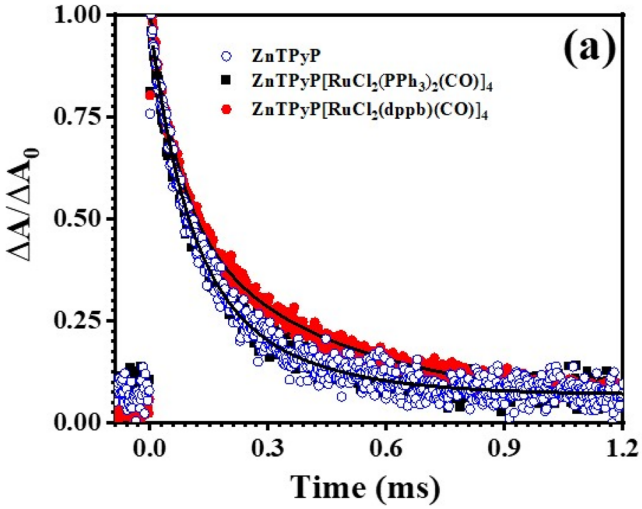


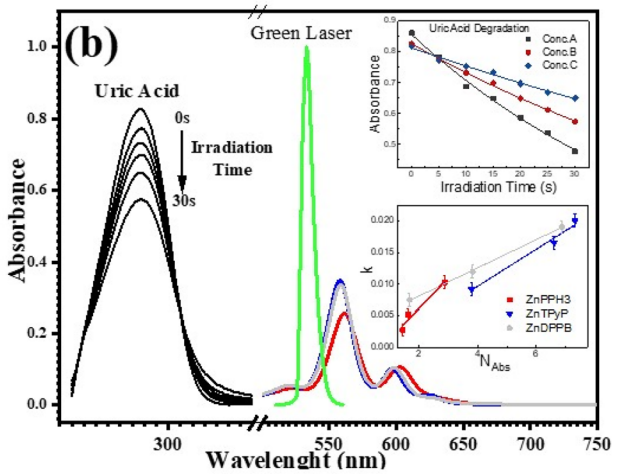


**Fig. 6** **a** Normalized transient absorption for ZnTPyP (open blue circles), ZnTPyP[$RuCl_2$(dppb)(CO)]$_4$ (full red circles), and ZnTPyP [$RuCl_2$ $(PPh_3)_2$(CO)]$_4$ (full black squarer). The black solid lines are the monoexponential fittings. **b** Q-band absorption spectra of ZnTPyP (solid blue lines), ZnTPyP[$RuCl_2$(dppb)(CO)]$_4$ (solid gray line), and ZnTPyP [$RuCl_2$ $(PPh_3)_2$(CO)]$_4$ (solid red line) along with the photodegradation of uric acid (UA) as a function of irradiation time (solid black line) and the emission spectrum of the excitation source (green laser with λexc = 532 nm, solid green line). Inserted in **b**, we have the dependence of UA absorbance at 290 nm as a function of the irradiation time for different concentrations (top panel), and the efficiency of $^1O_2$ formation (bottom panel)

outlying complexes in the porphyrin ring. This effect can be confirmed by understanding how such complexes are affecting the excited state triplet properties. We, therefore, measured the excited state relaxation time (via laser flash photolysis, see Fig. 6a) and the singlet oxygen quantum yield $\left(\Phi_{\Delta}\right)$ using uric acid as a scavenger (Fig. 6b). The obtained results are summarized in Table 3.

All the samples investigated in this work produce triplet states, and the presence of ruthenium complexes in the ZnTPyP structure increases the excited triplet state lifetime, see Table 3. Singlet oxygen is formed via an energy transfer process between the excited triplet state of zinc porphyrins and the molecular oxygen's ground state. Our results show that ZnTPyP[$RuCl_2(CO)(PPh_3)_2]_4$ presents a higher $\Phi_{\Delta}$ compared to that for ZnTPyP, while ZnTPyP[$RuCl_2$(dppb)$(CO)]_4$ presents a slightly lower $\Phi_{\Delta}$. It is important to note that the increase in the singlet oxygen production found in ZnTPyP[$RuCl_2(CO)(PPh_3)_2]_4$ could be explained by the reduction of fluorescence and internal conversion quantum yields in favor of the intersystem crossing process.

## 3 Conclusions

Summarizing, the spectroscopic properties of ZnTPyP, ZnTPyP[$RuCl_2$(dppb)$(CO)]_4$, and ZnTPyP[$RuCl_2(CO)(PPh_3)_2]_4$ are investigated, demonstrating that the ZnTPyP vibronic progressions, excited-state PESs, fluorescence quantum yields, and singlet excited-state deactivation pathways are significantly affected by the presence of the ruthenium outlying complexes. Such complexes are responsible for triggering additional non-radiative mechanisms in the relaxation pathways. Although ZnTPyP[$RuCl_2$(dppb)$(CO)]_4$ systems do not display any significant modification in their singlet states' relaxation pathways and the efficiency for generating singlet oxygen, ZnTPyP[$RuCl_2$ $(PPh_3)_2(CO)]_4$ systems present robust modifications on both properties, indicating the relevance of the ligands bonded to ruthenium complexes for the tunning of the porphyrin's photophysical properties.

## 4 Experimental

### 4.1 Sample Synthesis

The synthesis of ZnTPyP was accomplished following the procedures described in the literature [19]. The supramolecular porphyrins were synthesized under argon following the reaction of ZnTPyP with [$RuCl_2(PPh_3)_2(CO)$ (DMF)] or [$Ru_2Cl_4$(dppb)$_3(CO)_2$] to provide the ZnTPyP[$RuCl_2(PPh_3)_2(CO)]_4$ or ZnTPyP[$RuCl_2$(dppb)$(CO)]_4$, respectively. The solution was stirred for 4 h at room temperature, and the resulting solution was concentrated to approximately 90%, being ethyl ether added to produce a solid. The complex was collected by vacuum filtration, washed with ethyl ether, and dried under vacuum. The solutions were then filtered, and the resulting filter cake was washed with ethyl ether. The resultant powder was finally dried in a vacuum. In detail, (1) ZnTPyP[$RuCl_2(CO)(PPh_3)_2]_4$ were synthesized using 10 mg ($1.47\times10^{-5}$ mol) of ZnTPyP with 43.1 mg ($5.86\times10^{-5}$ mol) of [$RuCl_2(CO)(PPh_3)_2$(DMF)] in 20 mL of dichloromethane. Yield: 36.10% (19 mg); Exp. (Calc.), %C = 61.40 (61.36); %H = 3.98 (3.95); %N = 3.14 (3.03) and (2) ZnTPyP[$RuCl_2$(dppb)$(CO)]_4$ were synthesized using 10 mg ($1.47\times10^{-5}$ mol) of ZnTPyP with 61.3 mg ($2.94\times10^{-5}$ mol) of [$Ru_2Cl_4$(dppb)$_3(CO)_2$] in 20 mL of dichloromethane. Yield: 79.3% (33 mg); Exp. (Calc.), %C = 57.92 (58.77); %H = 4.51 (4.30); %N = 3.44 (3.52).

### 4.2 Spectroscopic Measurements

The spectroscopic measurements were performed at room conditions (temperature and pressure) with molecules completely dissolved in dimethylsulfoxide (DMSO), used as received from ISOFAR Inc., and placed in a quartz cuvette of 1.0 cm path length (four polished windows). A JASCO V-670 spectrophotometer was employed to acquire the steady-state absorbance spectra. To measure the steady-state fluorescence spectra, a setup composed of (1) Xenon lamp, (2) a monochromator model 300i from ACTON, and (3) a portable spectrophotometer from Ocean Optics was used. All samples were excited at the maximum of their respective B-bands. The supramolecules' emission quantum yield was estimated via the external reference method [55], taking ZnTPyP as the reference sample [54]. Time-resolved fluorescence experiments were performed with a *time-correlated single photon counting* (TCSPC) system from Horiba (Delta-Flex model, 27 ps per channel), equipped with a pulsed LED (excitation wavelength at 352 nm with 8 MHz of repetition rate) as the excitation source. The decays were collected at the maximum of the fluorescence spectra. Triplet excited state lifetime measurements were carried out via the laser flash photolysis technique using a frequency-doubled, Q-switched Quantel Brilliant pulsed Nd:YAG laser (532 nm, 10 Hz, 5 ns pulse width, 5 mJ) as the excitation source. In the experiments, the solution absorbance at the excitation wavelengths did not exceed $A = 0.2$. The decay curves of the transient absorption ($\Delta$A(t)) were registered by optical absorption at 470 nm.

### 4.3 Singlet Oxygen Quantum Yield

The singlet oxygen quantum yield $\left(\Phi_{\Delta}\right)$ were obtained by the indirect method using the uric acid (UA) as quencher scavenger [31, 56] and the *meso*-tetra(phenyl)porphyrin (TPP) as standard (TPP, $\Phi_{\Delta} = 0.52$ [57], in DMSO solution). The compounds solutions were prepared in three concentrations, while UA stayed at a fixed concentration. For each porphyrin

concentration, stirred solutions containing porphyrin and UA were irradiated in a cuvette (1.0 × 1.0 cm quartz cells) by a 532 nm laser (50 mW, the peak width $\Delta\lambda_{1/2} = 9$ nm).

The generation of singlet oxygen was quantified by monitoring the UA photodegradation through its absorption band (~290 nm) as a function of irradiation time [58]. The $\Phi_\Delta$ values were obtained using:

$$\Phi_\Delta = \Phi_\Delta^0 \frac{\gamma_\Delta}{\gamma_\Delta^0} \tag{1}$$

where "0" superscript labels are the parameters for the standard photosensitizer and $\gamma_\Delta$ is the efficiency of singlet oxygen formation, which is defined by:

$$\gamma_\Delta \propto \frac{k}{\mathrm{n_{abs}}} \tag{2}$$

being $k$ the UA's rate of photodegradation and $n_{abs}$ the number of absorbed photons per second. The $\mathrm{n_{abs}}$ is obtained by:

$$\mathrm{n_{abs}} = \frac{1}{\mathrm{hc}} \int_{\lambda_1}^{\lambda_2} \left(1 - 10^{-\mathrm{A}(\lambda)}\right) \mathrm{P}(\lambda) \mathrm{d}\lambda \tag{3}$$

In Eq. (3), $h$ is the Planck's constant, $c$ is the velocity of light, $A(\lambda)$ is the absorbance of the sample, and $P(\lambda)$ is the incident power. The integration limits were taken based on the porphyrin absorption and laser irradiation overlapping spectral interval.

**Acknowledgements** The authors are grateful to Prof. Sanclayton Moreira of the Graduate Program in Physics of the Federal University of Para for granting access to his experimental facilities.

**Funding** The Brazilian authors are indebted to the Brazilian National Council for Scientific and Technological Development (CNPq – processes numbers: 306147/2020-3 and 425124/2018-5), São Paulo Research Foundation (FAPESP – process number: 2014/50869-6), Fundação de Amparo à Pesquisa do Estado de Goiás (FAPEG – 201410267001776 and 201710267000533) and the Education Ministry (CAPES – Process number: 23038.000776/201754) via the projects of the National Institute for Science and Technology on Organic Electronics and with Amazonian Foundation for the Support of Studies and Research (FAPESPA – process number: 88881.159129/2017-01). N. M. B. N. is especially indebted to the Fulbright Foundation for its Visiting Professor Award Grant. This work is supported by the National Science Foundation under the CAREER grant # CHE-1848418.

## Declarations

**Conflict of Interest** The authors declare no competing interests.

## References

1. P.R. Kumar, N.J. Britto, A. Kathiravan, A. Neels, M. Jaccob, E.M. Mothi, New J. Chem. **43**(3), 1569–1580 (2019). https://doi.org/10.1039/C8NJ04289F
2. R. Hamze, S. Shi, S.C. Kapper, D.S. Muthiah Ravinson, L. Estergreen, M.-C. Jung, A.C. Tadle, R. Haiges, P.I. Djurovich, J.L. Peltier, R. Jazzar, G. Bertrand, S.E. Bradforth, M.E. Thompson, J. Am. Chem. Soc. **141**(21), 8616–8626 (2019)
3. T. Mede, M. Jäger, U.S. Schubert, Chem. Soc. Rev. **47**(20), 7577–7627 (2018). https://doi.org/10.1039/C8CS00096D
4. H.E. Toma, K. Araki, Exploring the supramolecular coordination chemistry-based approach for nanotechnology. In *Progress in Inorganic Chemistry*, vol. 56 (Wiley: Chichester, 2009)
5. N.M. Boyle, J. Rochford, M.T. Pryce, Coord. Chem. Rev. **254**(1), 77–102 (2010)
6. S. Allard, M. Forster, B. Souharce, H. Thiem, U. Scherf, Angew. Chem. **47**(22), 4070–4098 (2008)
7. Ö. Birel, S. Nadeem, H. Duman, J. Fluoresc. **27**(3), 1075–1085 (2017)
8. R.-B. Lin, S.-Y. Liu, J.-W. Ye, X.-Y. Li, J.-P. Zhang, Adv. Sci. **3**(7), 1500434 (2016)
9. L.K. McKenzie, H.E. Bryant, J.A. Weinstein, Coord. Chem. Rev. **379**, 2–29 (2019)
10. W. Li, Q. Xie, L. Lai, Z. Mo, X. Peng, E. Leng, D. Zhang, H. Sun, Y. Li, W. Mei, S. Gao, Photodiagn. Photodyn. Ther. **18**, 83–94 (2017)
11. S. Yano, S. Hirohara, M. Obata, Y. Hagiya, S.-I. Ogura, A. Ikeda, H. Kataoka, M. Tanaka, T.J. Joh, Photochem. Photobiol. C **12**(1), 46–67 (2011)
12. H. Dodziuk, *Introduction to supramolecular chemistry* (Kluwer Academic Publishers, Boston, 2002)
13. H.E. Toma, K. Araki, Coord. Chem. Rev. **196**(1), 307–329 (2000)
14. J.M.S. Lopes, K. Sharma, R.N. Sampaio, A.A. Batista, A.S. Ito, A.E.H. Machado, P.T. Araújo, N.B. Neto, M. Spectrochim. Acta A **209**, 274–279 (2019)
15. J.M.S. Lopes, R.N. Sampaio, A.S. Ito, A.A. Batista, A.E.H. Machado, P.T. Araujo, N.M.B. Neto, Spectrochim. Acta A **215**, 327–333 (2019)
16. J.M.S. Lopes, R.N. Sampaio, L.R. Dinelli, A.A. Batista, P.T. Araujo, N.M.B. Neto, Spectrochim. Acta A **224**, 117371 (2020)
17. P.J. Gonçalves, L.D. Boni, N.M.B. Neto, J.J. Rodrigues, S.C. Zílio, I.E. Borissevitch, Chem. Phys. Lett. **407**(1), 236–241 (2005)
18. E.S. Ryland, M.-F. Lin, M.A. Verkamp, K. Zhang, K. Benke, M. Carlson, J. Vura-Weis, J. Am. Chem. Soc. **140**(13), 4691–4696 (2018)
19. N.M. Barbosa Neto, L. De Boni, C.R. Mendonça, L. Misoguti, S.L. Queiroz, L.R. Dinelli, A.A. Batista, S.C. Zilio, J. Phys. Chem. B **109**(36), 17340–17345 (2005)
20. H.L. Kee, J. Bhaumik, J.R. Diers, P. Mroz, M.R. Hamblin, D.F. Bocian, J.S. Lindsey, D.J. Holten, Photochem. Photobiol. A **200**(2), 346–355 (2008)
21. A.K. Mandal, M. Taniguchi, J.R. Diers, D.M. Niedzwiedzki, C. Kirmaier, J.S. Lindsey, D.F. Bocian, D. Holten, J. Phys. Chem. A **120**(49), 9719–9731 (2016)
22. M.O. Senge, Chem. Comm. **47**(7), 1943–1960 (2011). https://doi.org/10.1039/C0CC03984E
23. R. Patra, A. Chaudhary, S.K. Ghosh, S.P. Rath, Inorg. Chem. **49**(5), 2057–2067 (2010)
24. A. Takahashi, D. Yamaki, K. Ikemura, T. Kurahashi, T. Ogura, M. Hada, H. Fujii, Inorg. Chem. **51**(13), 7296–7305 (2012)
25. Z. Yang, G. Pu, X. Ning, Y. Wu, Z. Zhang, D. Shan, X.-Q. Lu, Phys. Chem. Chem. Phys. (2019). https://doi.org/10.1039/C9CP01278H
26. P.D. Harvey, C. Stern, C.P. Gros, R. Guilard, Coord. Chem. Rev. **251**(3), 401–428 (2007)
27. Y. Kuramochi, Y. Kawakami, A. Satake, Inorg. Chem. **56**(18), 11008–11018 (2017)
28. A.L.A. Parussulo, B.A. Iglesias, H.E. Toma, K. Araki, Chem. Comm. **48**(55), 6939–6941 (2012). https://doi.org/10.1039/C2CC31173A
29. P. Cosma, L. Catucci, P. Fini, P.L. Dentuto, A. Agostiano, N. Angelini, L.M. Scolaro, Photochem. Photobiol. **82**(2), 563–569 (2006)

30. T. Gatti, P. Cavigli, E. Zangrando, E. Iengo, C. Chiorboli, M.T. Indelli, Inorg. Chem. **52**(6), 3190–3197 (2013)
31. P.J. Gonçalves, F.C. Bezzerra, A.V. Teles, L.B. Menezes, K.M. Alves, L. Alonso, A. Alonso, M.A. Andrade, I.E. Borissevitch, G.R.L. Souza, B.A. Iglesias, J. Photochem. Photobiol. A **391**, 112375 (2020)
32. N.M. Barbosa Neto, S.L. Oliveira, I. Guedes, L.R. Dinelli, L. Misoguti, C.R. Mendonça, A.A. Batista, S. Zílio, C. J. Braz. Chem. Soc. **17**(7), 1377–1382 (2006)
33. H.E. Toma, An. Acad. Bras. Ciênc. **72**(1), 5–25 (2000)
34. S. Majumder, B.P. Borah, J. Bhuyan, Dalton Trans. **49**(25), 8419–8432 (2020). https://doi.org/10.1039/D0DT00813C
35. K.E. Splan, M.H. Keefe, A.M. Massari, K.A. Walters, J.T. Hupp, Inorg. Chem. **41**(4), 619–621 (2002)
36. K. Kalyanasundaram, *Photochemistry of polypyridine and porphyrin complexes* (Academic Press, San Diego, 1992)
37. M. Gouterman, Optical spectra and electronic structure of porphyrins and related rings, in *The porphyrins*, vol. 3, ed. by D. Dolphin (Academic Press, Inc., 1978), pp. 1–156
38. U. Tripathy, R.P.J. Steer, Porphyr. Phthalocyanines **11**(04), 228–243 (2007)
39. J. Karolczak, D. Kowalska, A. Lukaszewicz, A. Maciejewski, R.P. Steer, J. Phys. Chem. A **108**(21), 4570–4575 (2004)
40. H.-Z. Yu, J.S. Baskin, A.H. Zewail, J. Phys. Chem. A **106**(42), 9845–9854 (2002)
41. C.M. Marian, Wiley Interdisciplinary Rev. Comput. Mol. Sci. **2**(2), 187–203 (2012)
42. M. Ethirajan, Y. Chen, P. Joshi, R.K. Pandey, Chem. Soc. Rev. **40**(1), 340–362 (2011). https://doi.org/10.1039/B915149B
43. F. Schmitt, P. Govindaswamy, G. Süss-Fink, W.H. Ang, P.J. Dyson, L. Juillerat-Jeanneret, B. Therrien, J. Med. Chem. **51**(6), 1811–1816 (2008)
44. A. Prodi, C.J. Kleverlaan, M.T. Indelli, F. Scandola, E. Alessio, E. Iengo, Inorg. Chem. **40**(14), 3498–3504 (2001)
45. A. Harriman, J. Chem. Soc. Faraday Trans. 2 **77**(7), 1281–1291 (1981). https://doi.org/10.1039/F29817701281
46. A. Prodi, M.T. Indelli, C.J. Kleverlaan, E. Alessio, F. Scandola, Coord. Chem. Rev. **229**(1), 51–58 (2002)
47. M. Gouterman, G.H. Wagnière, L.C. Snyder, J. Mol. Spectrosc. **11**(1), 108–127 (1963)
48. J.M. Lim, Z.S. Yoon, J.-Y. Shin, K.S. Kim, M.-C. Yoon, D. Kim, Chem. Comm. **3**, 273 (2008). https://doi.org/10.1039/B810718A
49. P.G. Seybold, M. Gouterman, J. Mol. Spectrosc. **31**(1), 1–13 (1969)
50. R.N. Sampaio, W.R. Gomes, D.M.S. Araujo, A.E.H. Machado, R.A. Silva, A. Marletta, I.E. Borissevitch, A.S. Ito, L.R. Dinelli, A.A. Batista, S.C. Zílio, P.J. Gonçalves, N.M. Barbosa Neto, J. Phys. Chem. A **116**(1), 18–26 (2012)
51. R.N. Sampaio, M.M. Silva, A.A. Batista, N.M.B. Neto, J. Photochem. Photobiol. A **315**, 98–106 (2016)
52. G. Lanzani, *The photophysics behind photovoltaics and photonics* (Wiley-VCH, Weinheim, 2012)
53. W.W. Parson, *Modern optical spectroscopy: with examples and exercises from biophysics and biochemistry* (Springer, Heildeberg, 2015)
54. K. Hirakawa, Y. Hosokawa, Y. Nishimura, S. Okazaki, Chem. Phys. Lett. **732**, 136652 (2019)
55. J.R. Lakowicz, *Principles of fluorescence spectroscopy*, 3rd edn. (Springer, New York, 2006)
56. É.R. Silva, A.L.S. Pavanelli, L.B. Mostaço, F.A. Schaberle, S.E. Galembeck, P.J. Gonçalves, R. Costa e Silva, L.P. Ferreira, T.D. Nekipelova, A.A. Kostyukov, A.S. Radchenko, A.A. Shtil, V.A. Kuzmin, I.E. Borissevitch, J. Photochem. Photobiol. A **349**, 42–48 (2017)
57. A.R. Silva, A.C. Pelegrino, A.C. Tedesco, R.A. Jorge, J. Braz. Chem. Soc. **19**(3), 491–501 (2008)
58. A.P. Gerola, J. Semensato, D.S. Pellosi, V.R. Batistela, B.R. Rabello, N. Hioka, W. Caetano, J. Photochem. Photobiol. A **232**, 14–21 (2012)